

Coupling and characterization of a Si/SiGe triple quantum dot array with a microwave resonator

Shun-Li Jiang(江顺利), Tian-Yi Jiang(蒋天翼), Yong-Qiang Xu(徐永强), Rui Wu(吴睿), Tian-Yue Hao(郝天岳), Shu-Kun Ye(叶澍坤), Ran-Ran Cai(蔡冉冉), Bao-Chuan Wang(王保传), Hai-Ou Li(李海欧), Gang Cao(曹刚), and Guo-Ping Guo(郭国平)

Citation: Chin. Phys. B, 2024, 33 (**9**): 090311. DOI: 10.1088/1674-1056/ad711d
Journal homepage: http://cpb.iphy.ac.cn; http://iopscience.iop.org/cpb

What follows is a list of articles you may be interested in

Enhancing quantum temporal steering via frequency modulation

Mengkai Wu(吴孟凯) and Weiwen Cheng(程维文)
Chin. Phys. B, 2024, 33 (**5**): 050306. DOI: 10.1088/1674-1056/ad2505

Ascertaining the influences of auxiliary qubits on the Einstein-Podolsky-Rosen steering and its directions

Ling-Ling Xing(邢玲玲), Huan Yang(杨欢), Gang Zhang(张刚), and Min Kong(孔敏)
Chin. Phys. B, 2024, 33 (**5**): 050304. DOI: 10.1088/1674-1056/ad1927

Broadband multi-channel quantum noise suppression and phase-sensitive modulation based on entangled beam

Ke Di(邸克), Shuai Tan(谈帅), Anyu Cheng(程安宇), Yu Liu(刘宇), and Jiajia Du(杜佳佳)
Chin. Phys. B, 2023, 32 (**10**): 100302. DOI: 10.1088/1674-1056/acd8a8

Quantum interferometric power and non-Markovianity in the decoherence channels

Shaojie Xiong(熊少杰), Zhe Sun(孙哲), and Xiaoguang Wang(王晓光)
Chin. Phys. B, 2023, 32 (**8**): 080302. DOI: 10.1088/1674-1056/accb4e

Circuit quantum electrodynamics with a quadruple quantum dot

Ting Lin(林霆), Hai-Ou Li(李海欧), Gang Cao(曹刚), and Guo-Ping Guo(郭国平)
Chin. Phys. B, 2023, 32 (**7**): 070307. DOI: 10.1088/1674-1056/accd57

SPECIAL TOPIC — Quantum computing and quantum sensing

Coupling and characterization of a Si/SiGe triple quantum dot array with a microwave resonator

Shun-Li Jiang(江顺利)[1,2], Tian-Yi Jiang(蒋天翼)[1,2], Yong-Qiang Xu(徐永强)[1,2], Rui Wu(吴睿)[1,2], Tian-Yue Hao(郝天岳)[1,2], Shu-Kun Ye(叶澍坤)[1,2], Ran-Ran Cai(蔡冉冉)[1,2], Bao-Chuan Wang(王保传)[1,2], Hai-Ou Li(李海欧)[1,2], Gang Cao(曹刚)[1,2,†], and Guo-Ping Guo(郭国平)[1,2,3]

[1] *CAS Key Laboratory of Quantum Information, University of Science and Technology of China, Hefei* 230026, *China*
[2] *CAS Center for Excellence in Quantum Information and Quantum Physics, University of Science and Technology of China, Hefei* 230026, *China*
[3] *Origin Quantum Computing Company Limited, Hefei* 230088, *China*

(Received 16 June 2024; revised manuscript received 16 August 2024; accepted manuscript online 20 August 2024)

Scaling up spin qubits in silicon-based quantum dots is one of the pivotal challenges in achieving large-scale semiconductor quantum computation. To satisfy the connectivity requirements and reduce the lithographic complexity, utilizing the qubit array structure and the circuit quantum electrodynamics (cQED) architecture together is expected to be a feasible scaling scheme. A triple-quantum dot (TQD) coupled with a superconducting resonator is regarded as a basic cell to demonstrate this extension scheme. In this article, we investigate a system consisting of a silicon TQD and a high-impedance TiN coplanar waveguide (CPW) resonator. The TQD can couple to the resonator via the right double-quantum dot (RDQD), which reaches the strong coupling regime with a charge–photon coupling strength of $g_0/(2\pi) = 175$ MHz. Moreover, we illustrate the high tunability of the TQD through the characterization of stability diagrams, quadruple points (QPs), and the quantum cellular automata (QCA) process. Our results contribute to fostering the exploration of silicon-based qubit integration.

Keywords: triple-quantum dot, strong coupling, circuit quantum electrodynamics (cQED), scalable silicon-based cQED architectures

PACS: 03.67.Lx, 42.50.Wk, 68.65.Hb, 42.60.Da **DOI:** 10.1088/1674-1056/ad711d

1. Introduction

The exceptional desirability of silicon quantum dots arises from their impressive characteristics, including long coherence time and high operation fidelity,[1–3] which make them promising candidates for quantum computation applications. Considering that single- and two-qubit gates have been achieved with fidelity exceeding the surface code threshold in silicon,[4–6] there is increasing interest in qubit scaling architecture.[7–11] Circuit quantum electrodynamics (cQED) provides a leading platform for coupling qubits at a distance.[12–22] In such a system, microwave photons can mediate long-range qubit interactions, which requires strong coupling for efficient information exchange between photons and qubits.[23,24] By virtue of the high-impedance superconducting resonator,[23,25] previous works have successfully achieved strong coupling between photons and charge qubits.[23,24] Furthermore, the charge–spin hybridization achieved through spin–orbit coupling or micromagnets offers an approach to coupling spin qubits to photons. In this context, a flopping mode qubit is proposed, encoded in a double-quantum dot (DQD), and has achieved indirect coupling between the spin qubit and the resonator.[26–31] In addition, long-range qubit interactions mediated by both real[16] and virtual photons[19,32] have also been demonstrated.

Connecting separated qubit arrays through a resonator is an attractive approach for further qubit extension, which allows coherent information exchange between these arrays. In a quantum dot array, with the help of the flopping mode qubit, the DQD can be used to couple microwave photons with large coupling strength. And each of the remaining quantum dots can encode a single spin Loss–DiVincenzo (LD) qubit.[33] Considering that a triple-quantum dot (TQD) can form an LD and a flopping mode qubit, thus a resonator-coupled TQD system is the minimum cell for constructing a large-scale architecture based on cQED. This approach offers the advantage of allowing qubit arrays to be separated over a long distance, enabling a more efficient electrode arrangement and reducing unwanted thermal dissipation.[7] However, due to the difficulty of device fabrication, such systems have rarely been studied in silicon.

In this work, we fabricate a hybrid device consisting of the Si/SiGe TQD and a high-impedance coplanar waveguide (CPW) superconducting TiN resonator. Strong coupling between the charge qubit in the right quantum dot (RDQD) and the resonator photons is observed in the single electron regime. To demonstrate the tunability of the TQD, we tune the electrochemical potential of each quantum dot specifically, and ob-

†Corresponding author. E-mail: gcao@ustc.edu.cn

© 2024 Chinese Physical Society and IOP Publishing Ltd

serve two quadruple points (QPs) and quantum cellular automata (QCA) phenomena. With the Hubbard model[34] and the input–output theory,[35] the simulation diagram is provided and agrees well with the experimental data. These results indicate the potential of a qubit array coupled with resonator for scaling-up qubits.

2. Resonator-coupled triple-quantum dot device

The hybrid device investigated in our experiments is depicted in Fig. 1(a), comprising a high-impedance CPW resonator and two TQDs fabricated on a Si/SiGe heterostructure. The device is cooled to a base temperature of approximately 12 mK in a dilution refrigerator, and all experiments are performed in the left TQD (LTQD). As shown in Fig. 1(b), with different colors, three layers of Al electrodes are patterned using standard electron beam lithography (EBL). Each layer of the electrodes is insulated through a thermal process with oxygen plasma in atomic layer deposition (ALD). These electrodes are employed to construct the overlapping gate structure, defining the three quantum dots that are formed below the plunger gates P1, P2 and P3. They are labeled QD1, QD2 and QD3, respectively. For convenience, QD1 combined with QD2 is denoted as the left DQD (LDQD), while QD2 with QD3 is denoted as the right DQD (RDQD) in the following text. Here, the plunger gate P3 is connected to the anti-node of the resonator and DC biased via a pad to control its voltage.

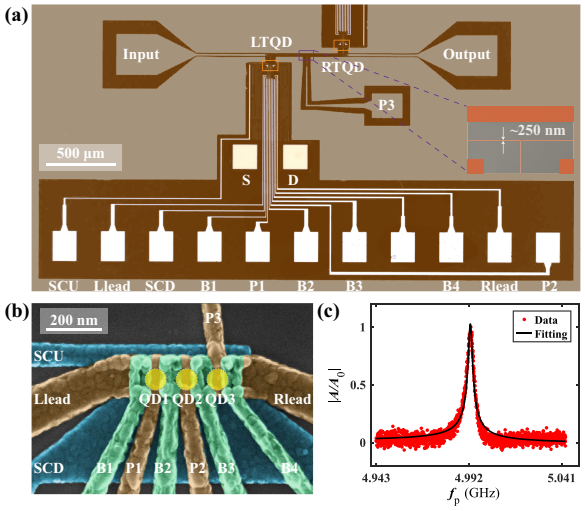


Fig. 1. Device structure in our experiment. (a) Optical image of the superconducting microwave resonator and two TQDs system. The inset shows the scanning electron microscope (SEM) image of a segment of the TiN resonator, of which the slot and center conductor width are 20 μm and 250 nm, respectively. (b) False-color SEM of the TQD. Electrodes are labeled SCU, Llead, SCD, B1, P1, B2, P2, B3, P3, B4 and Rlead. P1, P2 and P3 are plunger gates to control chemical potentials of each dot; B1, B2, B3 and B4 are barrier gates used to control the tunnel coupling between neighboring quantum dots or between the quantum dot and its adjacent reservoir. (c) Normalized resonator transmission amplitude A/A_0 as a function of probe frequency f_p before inducing any electrons to the TQD. The red dot-line shows the experimental data of the resonator, and the black line is the fitting result, from which an external background has been subtracted.

The resonator is fabricated with a 10 nm high kinetic-inductance TiN material thin film.[36] A vector network analyzer (VNA) is used to measure the transmission signal of the resonator. Fitting the transmission data in Fig. 1(c) to the Lorentzian curve corrected by the Fano effect,[37,38] we determine that center frequency $f_r = 4.993$ GHz and the decay rate of the resonator $\kappa/(2\pi) = 2.2$ MHz. The characteristic impedance is then estimated to be $Z_r \approx 3.5$ kΩ. In the following, the resonator is driven by a probe tone at frequency $f_p = f_r$ to detect the TQD charge states.

3. Strong coupling of the charge qubit and resonator

The strong coupling regime is a hallmark of the cQED system, where the coherent coupling rate $2g_0/(2\pi)$ between the qubit and the resonator photon exceeds both the qubit decoherence rate $\gamma/(2\pi)$ and the photon loss rate $\kappa/(2\pi)$.[39] In this section, we focus on the single-electron regime in the RDQD and characterize the coupling strength between the charge qubit and photons in the high-impedance resonator. In the following, we fix the probe power to the resonator at $P \approx -130$ dBm, corresponding to approximately two photons,[40] which enhances the signal-to-noise ratio compared to single photon. By setting the voltage of the B2 gate at 300 mV, the DQD stability diagram is clearly shown in Fig. 2(a), in which the normalized resonator transmission amplitude A/A_0 is plotted as a function of the gate voltages V_{P2} and V_{P3}. In this diagram, the charge states are labeled (N_2, N_3), where N_2 (N_3) represents the electron number in QD2 (QD3). When electrons tunnel between different charge states, the resonator transmission amplitude A/A_0 is reduced. Then, by tuning the B2 gate voltage to 90 mV, an obvious inter-dot transition line is depicted in Fig. 2(b), corresponding to the $(1,0) \leftrightarrow (0,1)$ transition, and these two states facilitate a charge qubit. The qubit frequency is $\omega_q = \sqrt{\varepsilon^2 + (2t_c)^2}$, where ε and $2t_c$ are qubit detuning and tunneling coupling of the quantum dots, respectively. As indicated by the yellow arrow in Fig. 2(b), the qubit detuning ε can be adjusted as a function of V_{P2} and V_{P3}. Subsequently, we slightly adjust the B2 gate voltage to 100 mV, with a tunneling coupling strength fitted approximately $2t_c \approx 2.7$ GHz. By scanning the detuning (we only adjust V_{P2} to simplify the experiment) and monitoring the resonator transmission spectrum, the vacuum Rabi splitting is illustrated in Fig. 2(c), proving the achievement of strong coupling.

To quantitatively determine the coupling strength and the qubit decoherence rate, we extract the resonance frequency $\tilde{\omega}$ and linewidth $\tilde{\kappa}$ for different qubit detunings by fitting with the Lorentzian line shape. The data are presented in Figs. 2(d) and 2(e) with red dots. According to the Jaynes–Cummings

model, the resonance frequency and linewidth satisfy the following equations:[23,41]

$$\tilde{\omega}_{\pm} = \omega_{\mathrm{r}} \pm \frac{1}{2}\sqrt{4g^2 + (\omega_{\mathrm{r}} - \omega_{\mathrm{q}})^2},$$
$$\tilde{\kappa}_{\pm} = \gamma + \frac{\kappa}{2} \mp \left(\gamma - \frac{\kappa}{2}\right)\cos\theta,$$

where ω_{r} is the resonator frequency, $g = g_0 \frac{2t_{\mathrm{c}}}{\omega_{\mathrm{q}}}$ is the effective coupling strength, $\gamma/(2\pi)$ represents the qubit decoherence rate and $\theta = (1/2)\tan^{-1}\left(\frac{2g}{\omega_{\mathrm{q}} - \omega_{\mathrm{r}}}\right)$. Fitting the data to the equations, we obtain the coupling strength $g_0/(2\pi) = 175$ MHz and the qubit decoherence rate $\gamma/(2\pi) = 99$ MHz. Additionally, using the input–output theory,[35] the simulation of vacuum Rabi splitting in Fig. 2(f) corresponds well to that in Fig. 2(c).

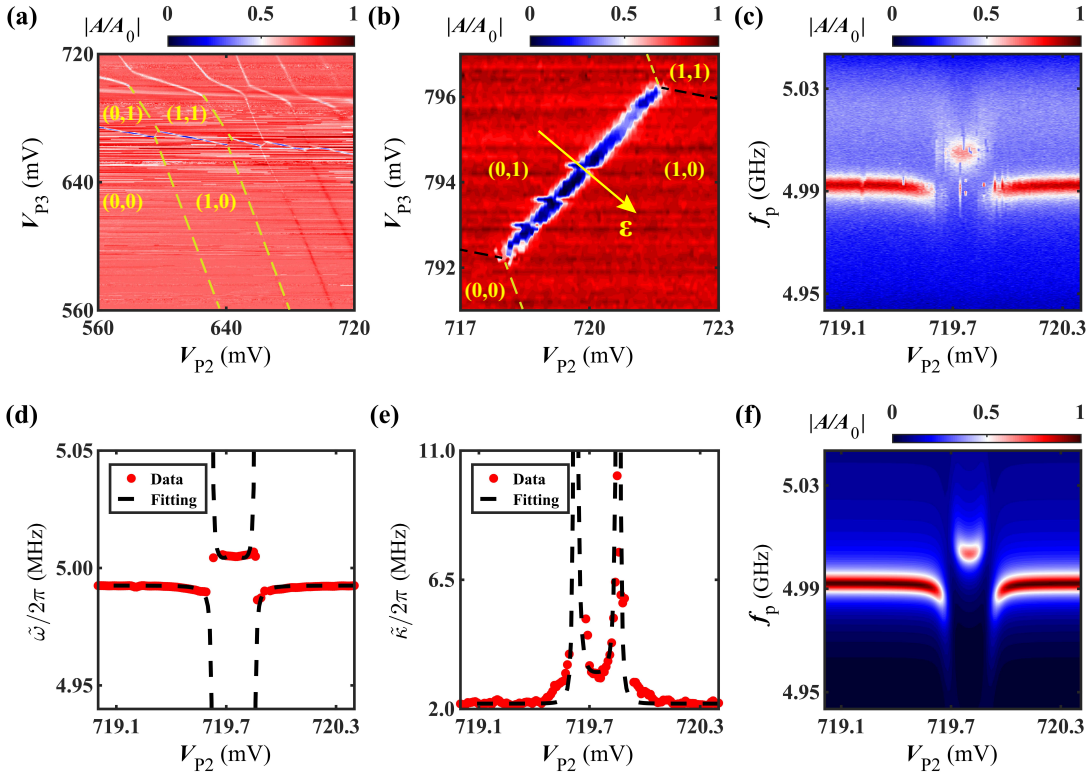


Fig. 2. DQD properties and the vacuum Rabi splitting. (a) Stability diagrams of RDQD with the left quantum dot QD1 served as an extended reservoir. The electron numbers are labeled in the figure. (b) Resonator transmission in the vicinity of the $(0,1) \leftrightarrow (1,0)$ interdot charge transition. A small background is subtracted from each horizontal line of the data set in (a) and (b). (c) Resonator transmission spectrum as a function of f_{p} and V_{P2}. The vacuum Rabi splitting, as a hallmark of strong coupling, is observed for charge qubit in the RDQD. (d) and (e) The extracted frequency $\tilde{\omega}$ and the linewidth $\tilde{\kappa}$ as a function of the voltage V_{P2}, respectively (red dots). The black dashed line curves in panels (d) and (e) are fitted by the Jaynes–Cummings model. (f) Simulation of the vacuum Rabi splitting using the input–output theory.[35] In this simulation, $g_0/(2\pi) = 175$ MHz, $\gamma/(2\pi) = 99$ MHz, $2t_{\mathrm{c}}/(2\pi) = 2.67$ GHz and lever arm $\alpha = 150$ meV/V.

4. Characterization of triple-quantum dot

To demonstrate that the TQD is a qualified local module, verifying the tunability of each quantum dot is of great importance.[42] By investigating the specific transport phenomena (QCA and QPs), we characterize the tunability of our TQD and demonstrate it as a well-controlled quantum dot array. The electron tunneling in the TQD is detected by monitoring the resonator response while scanning the voltage of gates P1 and P3, with the voltage of gate P2 fixed at $V_{\mathrm{P2}} = 840$ mV. By operating in the dispersive region, the stability diagram of the TQD, characterized by the resonator phase shift, is clearly shown in Fig. 3(a). The electron occupation state in the TQD is labeled (N_1, N_2, N_3), where N_1, N_2 and N_3 are the electron numbers in QD1, QD2 and QD3, respectively. Three charging lines with different negative slopes emerge, corresponding to the processes in which electrons in three different dots tunnel through the source/drain reservoir. In Fig. 3(a), a particular region where three different charging lines converge is observed in the upper right corner (black dashed rectangle). To analyze the evolution of this region more precisely, we keep the voltage of gate P2 constant, slightly adjust the barrier voltage, and perform measurement with smaller scan interval, as shown in Fig. 3(b). In this region, eight triple points labeled A–H are observed, which are the degenerate points of three different electron states,[43] and these triple points form a quadrilateral (area I in Fig. 3(b)) and a hexagon (area II) in the stability diagram. The energy levels of the triple points are shown in Fig. 3(c), and we find that there are four types of them. For example, at triple point B, the energy level of the source reservoir is aligned with that of QD1, and the energy level of QD2 is

aligned with that of QD3, corresponding to the intersection of three charge states $(1,4,4)$, $(1,5,3)$ and $(2,4,4)$ in Fig. 3(b).

In the TQD system, the sequential tunneling process only occurs at QPs,[44] where four charge configuration states are energy degenerate. By carefully tuning the voltage of P2 to $V_{P2} = 842$ mV and slightly adjusting the voltages of B3 and B4, triple points B (D) and E (F) merge into QP α (β), as shown in Fig. 3(d). These QPs contain the following degenerate charge states:

$$\alpha : (1,4,4) \leftrightarrow (2,4,4) \leftrightarrow (1,5,4) \leftrightarrow (1,5,3),$$
$$\beta : (1,5,3) \leftrightarrow (2,5,3) \leftrightarrow (2,4,4) \leftrightarrow (2,4,3).$$

The energy levels of the QPs are shown in Fig. 3(f), of which all the quantum dots are matched to the source and drain reservoirs. Thus, sequential tunneling processes can occur in these configurations. Additionally, in Fig. 3(d), a negative slope line connecting α and β is located between two charge-stable areas (1,5,3) and (2,4,4), indicating a joint process. This is a second order co-tunneling process, in which an electron from an outside quantum dot is added to or removed from a reservoir, and another electron tunnels between the other two dots automatically, this is called the QCA process.[43,45] Utilizing the Hubbard model to characterize the transport processes of the TQD[46] and the input–output theory to describe the resonator responses,[35] we simulate the result in Fig. 3(e), which matches the experimental data quite well.

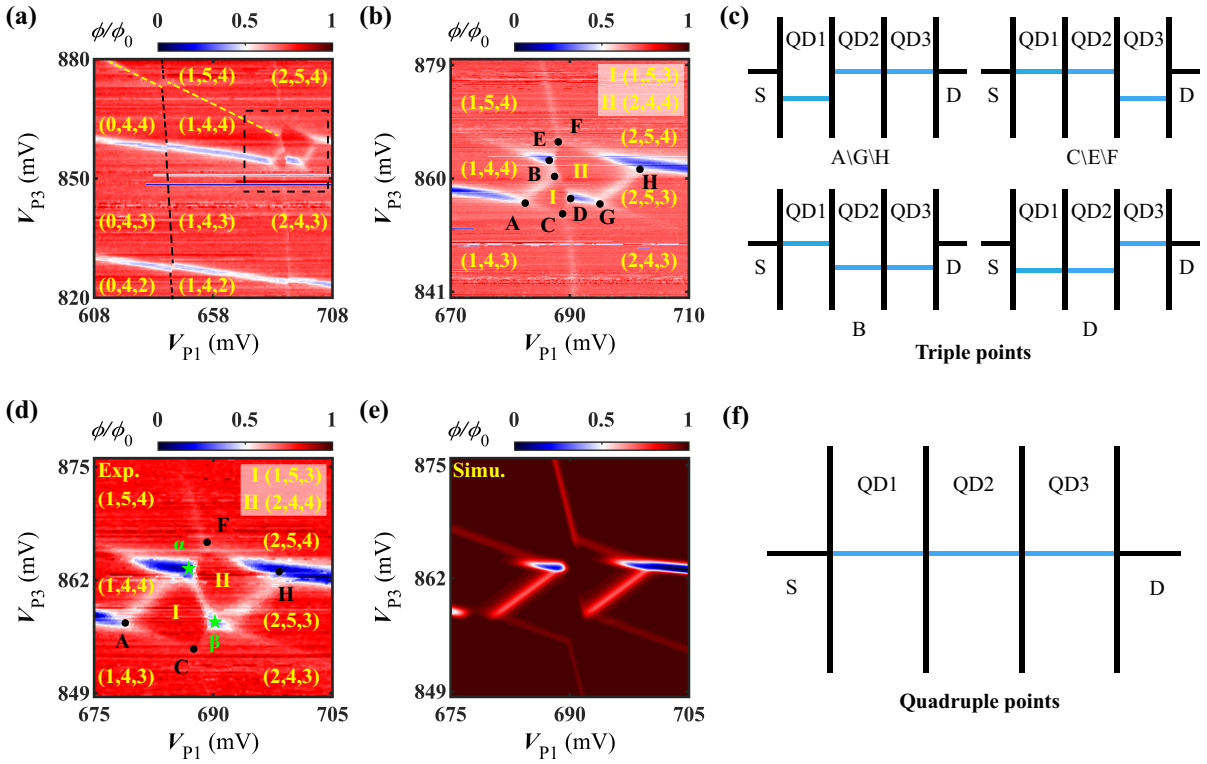


Fig. 3. Tunability of the TQD properties. (a) The typical TQD charge stability diagram. For a given voltage of gate P2, three charging lines with different slopes can be obtained by scanning the voltages of gates P1 and P3. The black/yellow dashed line here means the transition line between QD1/QD2 and the reservoir. (b) The TQD charge stability diagram with 8 triple points, which are indicated by black circle with A–H. (c) The energy levels sketch of eight triple points of the TQD, where S and D are source and drain reservoirs of the TQD, respectively. (d) The TQD charge stability diagram with QPs α and β, indicated by stars where four charging lines intersect. (e) Simulation result for (d). (f) The energy level sketch of the TQD in the case of quadruple points.

5. Conclusion

In summary, we investigate the hybrid system of a Si/SiGe TQD coupled with a microwave resonator and successfully illustrate the strong coupling of a charge qubit in the RDQD and the microwave photon. In addition, we explore the transport characteristics of the TQD system using a resonator. Our study demonstrates the evolution from a basic stability diagram to two unique transport phenomena: QP and QCA. These results suggest that we have achieved coupling between the quantum dot array and the resonator.

In such highly tunable TQD, a flopping mode spin qubit can be encoded in the DQD connected to the resonator, and an LD spin qubit will be encoded in the third quantum dot. The flopping mode qubit can act as a mediator, facilitating the coupling of the single spin qubit to the resonator. This capability holds considerable potential, as long-distance quantum information exchange between quantum dot arrays could be enabled by combining the spin exchange interactions and spin-shuttling technique.[47] Our work makes a step towards scalable quantum computing architectures.

Acknowledgments

Project supported by the National Natural Science Foundation of China (Grant Nos. 92265113, 12074368, 12304560, and 12034018) and China Postdoctoral Science Foundation (Grant Nos. BX20220281 and 2023M733408). This work was partially carried out at the USTC Center for Micro- and Nanoscale Research and Fabrication.

References

[1] Simmons C B, Prance J R, Bael B J V, Koh T S, Shi Z, Savage D E, Lagally M G, Joynt R, Friesen M, Coppersmith S N and Eriksson M A 2011 *Phys. Rev. Lett.* **106** 156804
[2] Veldhorst M, Hwang J C C, Yang C H, Leenstra A W, de Ronde B, Dehollain J P, Muhonen J T, Hudson F E, Itoh K M, Morello A and Dzurak A S 2014 *Nat. Nanotechnol.* **9** 981
[3] Yoneda J, Takeda K, Otsuka T, Nakajima T, Delbecq M R, Allison G, Honda T, Kodera T, Oda S, Hoshi Y, Usami N, Itoh K M and Tarucha S 2018 *Nat. Nanotechnol.* **13** 102
[4] Xue X, Russ M, Samkharadze N, Undseth B, Sammak A, Scappucci G and Vandersypen L M K 2022 *Nature* **601** 343
[5] Mills A R, Guinn C R, Gullans M J, Sigillito A J, Feldman M M, Nielsen E and Petta J R 2022 *Sci. Adv.* **8** eabn5130
[6] Noiri A, Takeda K, Nakajima T, Kobayashi T, Sammak A, Scappucci G and Tarucha S 2022 *Nature* **601** 338
[7] Vandersypen L M K, Bluhm H, Clarke J S, Dzurak A S, Ishihara R, Morello A, Reilly D J, Schreiber L R and Veldhorst M 2017 *npj Quantum Inf.* **3** 34
[8] Gonzalez-Zalba M F, de Franceschi S, Charbon E, Meunier T, Vinet M and Dzurak A S 2021 *Nat. Electron.* **4** 872
[9] Philips S G J, Madzik M T, Amitonov S V, de Snoo S L, Russ M, Kalhor N, Volk C, Lawrie W I L, Brousse D, Tryputen L, Wuetz B P, Sammak A, Veldhorst M, Scappucci G and Vandersypen L M K 2022 *Nature* **609** 919
[10] Lin T, Li H O, Cao G and Guo G P 2023 *Chin. Phys. B* **32** 070307
[11] Xue R, Beer M, Seidler I, Humpohl S, Tu J S, Trellenkamp S, Struck T, Bluhm H and Schreiber L R 2024 *Nat. Commun.* **15** 2296
[12] Srinivasa V, Taylor J M and Tahan C 2016 *Phys. Rev. B* **94** 205421
[13] Nicolí G, Ferguson M S, Rössler C, Wolfertz A, Blatter G, Ihn T, Ensslin K, Reichl C, Wegscheider W and Zilberberg O 2018 *Phys. Rev. Lett.* **120** 236801
[14] Van Woerkom D, Scarlino P, Ungerer J, Müller C, Koski J, Landig A, Reichl C, Wegscheider W, Ihn T, Ensslin K and Wallraff A 2018 *Phys. Rev. X* **8** 041018
[15] Warren A, Barnes E and Economou S E 2019 *Phys. Rev. B* **100** 161303
[16] Borjans F, Croot X G, Mi X, Gullans M J and Petta J R 2020 *Nature* **577** 195
[17] Wang B C, Lin T, Li H O, Gu S S, Chen M B, Guo G C, Jiang H W, Hu X D, Cao G and Guo G P 2021 *Sci. Bull.* **66** 332
[18] Young S M, Jacobson N T and Petta J R 2022 *Phys. Rev. Appl.* **18** 064082
[19] Harvey-Collard P, Dijkema J, Zheng G, Sammak A, Scappucci G and Vandersypen L M K 2022 *Phys. Rev. X* **12** 021026
[20] Xu Y Q, Gu S S, Lin T, Wang B C, Li H O, Cao G and Guo G P 2023 *Sci. China-Phys. Mech. Astron.* **66** 237301
[21] Pan X, Song P and Y Gao Y 2023 *Chin. Phys. Lett.* **40** 110303
[22] Zhao C, He Y, Geng X, He K, Dai G, Liu J and Chen W 2022 *Chin. Phys. Lett.* **40** 010301
[23] Stockklauser A, Scarlino P, Koski J V, Gasparinetti S, Andersen C K, Reichl C, Wegscheider W, Ihn T, Ensslin K and Wallraff A 2017 *Phys. Rev. X* **7** 011030
[24] Scarlino P, van Woerkom D J, Mendes U C, Koski J V, Landig A J, Andersen C K, Gasparinetti S, Reichl C, Wegscheider W, Ensslin K, Ihn T, Blais A and Wallraff A 2019 *Nat. Commun.* **10** 3011
[25] Samkharadze N, Bruno A, Scarlino P, Zheng G, DiVincenzo D P, DiCarlo L and Vandersypen L M K 2016 *Phys. Rev. Appl.* **5** 044004
[26] Samkharadze N, Zheng G, Kalhor N, Brousse D, Sammak A, Mendes U C, Blais A, Scappucci G and Vandersypen L M K 2018 *Science* **359** 1123
[27] Mi X, Benito M, Putz S, Zajac D M, Taylor J M, Burkard G and Petta J R 2018 *Nature* **555** 599
[28] Benito M, Croot X, Adelsberger C, Putz S, Mi X, Petta J R and Burkard G 2019 *Phys. Rev. B* **100** 125430
[29] Croot X, Mi X, Putz S, Benito M, Borjans F, Burkard G and Petta J R 2020 *Phys. Rev. Research* **2** 012006
[30] Mutter P M and Burkard G 2021 *Phys. Rev. Research* **3** 013194
[31] Yu C X, Zihlmann S, Abadillo-Uriel J C, Michal V P, Rambal N, Niebojewski H, Bedecarrats T, Vinet M, Dumur É, Filippone M, Bertrand B, De Franceschi S, Niquet Y M and Maurand R 2023 *Nat. Nanotechnol.* **18** 741
[32] Dijkema J, Xue X, Harvey-Collard P, Rimbach-Russ M, de Snoo S L, Zheng G, Sammak A, Scappucci G and Vandersypen L M K 2023 arXiv: 2310.16805v1[quant–ph]
[33] Loss D and DiVincenzo D P 1998 *Phys. Rev. A* **57** 120
[34] Das Sarma S, Wang X and Yang S 2011 *Phys. Rev. B* **83** 235314
[35] Benito M, Mi X, Taylor J M, Petta J R and Burkard G 2017 *Phys. Rev. B* **96** 235434
[36] Amin K R, Ladner C, Jourdan G, Hentz S, Roch N and Renard J 2022 *Appl. Phys. Lett.* **120** 164001
[37] Kroner M, Govorov A O, Remi S, Biedermann B, Seidl S, Badolato A, Petroff P M, Zhang W, Barbour R, Gerardot B D, Warburton R J and Karrai K 2008 *Nature* **451** 311
[38] Miroshnichenko A E, Flach S and Kivshar Y S 2010 *Rev. Mod. Phys.* **82** 2257
[39] Mi X, Cady J V, Zajac D M, Deelman P W and Petta J R 2017 *Science* **355** 156
[40] Bϕttcher C G L, Harvey S P, Fallahi S, Gardner G C, Manfra M J, Vool U, Bartlett S D and Yacoby A 2022 *Nat. Commun.* **13** 4773
[41] Blais A, Huang R S, Wallraff A, Girvin S M and Schoelkopf R J 2004 *Phys. Rev. A* **69** 062320
[42] Li R, Petit L, Franke D P, Dehollain J P, Helsen J, Steudtner M, Thomas N K, Yoscovits Z R, Singh K J, Wehner S, Vandersypen L M K, Clarke J S and Veldhorst M 2018 *Sci. Adv.* **4** eaar3960
[43] Weijie L, Zhihai L, Jingwei M, Yi L, Dong P, Jianhua Z and Q X H 2023 *Adv. Quantum Technol.* **6** 2200158
[44] Rogge M C and Haug R J 2009 *New J. Phys.* **11** 113037
[45] Amlani I I, Orlov A O, Toth G, Bernstein G H, Lent C S and Snider G L 1999 *Science* **284** 289
[46] Russ M, Peterfalvi C G and Burkard G 2020 *J. Phys.: Condens. Matter* **32** 165301
[47] Mills A, Zajac D, Gullans M and Schupp F 2019 *Nat. Commun.* **10** 1063